Effects of hydrogen bond and solvent polarity on the C=O stretching of bis(2-thienyl)ketone in solution

Huigang Wang,[1,2,3,4,a)] Libo Wang,[1,2] Shaosong Shen,[1,2] Wenfei Zhang,[1,2] Mingde Li,[3] Lili Du,[3] Xuming Zheng,[1,2,b)] and David Lee Phillips[3]
[1]*Department of Chemistry and State Key Laboratory of Advanced Textiles Materials and Manufacture Technology, MOE, Zhejiang Sci-Tech University, Hangzhou 310018, China*
[2]*Engineering Research Center for Eco-dyeing and Finishing of Textiles, MOE, Zhejiang Sci-Tech University, Hangzhou 310018, China*
[3]*Department of Chemistry, The University of Hong Kong, Pokfulam Road, Hong Kong*
[4]*Department of Physics, University of Osnabrueck, 49069 Osnabrueck, Germany*

(Received 15 December 2011; accepted 6 March 2012; published online 28 March 2012)

The optimized structural parameters, the absorption and the resonance Raman spectra have been investigated for the bis(2-thienyl)ketone in gas phase, in cyclohexane, methanol, and acetonitrile solvents by means of time dependent density functional theory calculations, the solvent electronic polarization effect on the solvation shift is examined and in well accordance with the calculation. The effect of increasing the polarity of the solvent is well represented by the polarizable continuum model, both for the absorption spectra and resonance Raman intensities. The Raman spectra of the C=O stretching mode, which is sensitive to the intermolecular interaction for bis(2-thienyl)ketone dissolved in solvents, were systematically studied. It was found that the hydrogen bond effect plays an important role in reducing the carbonyl stretching wavenumbers. The results of Raman shifts were interpreted through the dilution effect, solvation effects, and hydrogen bond-forming effects. Furthermore, the excitation profiles of several important Raman bands of bis(2-thienyl)ketone molecule in different solvents have been critically analyzed. The solvent effects on structural and symmetry properties of the molecule in S2 electronic state as well as the short-time photo relaxation dynamics have been discussed. © *2012 American Institute of Physics*. [http://dx.doi.org/10.1063/1.3697482]

I. INTRODUCTION

Binding of biological macromolecules through weak, non-covalent interactions is critical for living organisms. It occurs in all kinds of biological structures.[1] Weak interactions, including Hydrogen bonding, Hydrophobic and hydrophilic interactions, protein–ligand and protein–DNA interactions, solvent polarization interactions, etc., have been well characterized and widely investigated in biological system.[1–3]

Vibrational spectroscopy is well-suited for the study of weak binding interactions, since the peak shape, frequency, and the intensity pattern of the C=O and amide I vibrational bands (peptide structure) are sensitively dependent on hydrogen bonding interaction between polypeptides or proteins and surrounding protic solvent molecules[4–6] and consequently allows the investigation of the secondary structure of proteins at different environment and to follow structural changes that occur during the solvent or polarity transition. A number of groups have investigated the interaction between C=O group and solvent polarity using Raman and infrared spectroscopy. Zhao *et al.*[3,7] had a systematic investigation of hydrogen bonding structures and dynamics in electronic excited states for a number of hydrogen-bonded systems using combined femtosecond time-resolved spectroscopy and accurate excited-state electronic structure calculations. They found that the intermolecular hydrogen-bond strengthening and weakening correspond to redshifts and blueshifts, respectively, in the electronic spectra. This is a guide for understanding spectra for variety of compounds, including our findings in this article. Hudson's[4] and Asher's[5,6] group reported a systematic investigation of the solvatochromic amide I mode frequency shift of the N-methylacetamide (NMA) in a variety of aprotic and protic solvents both in experimentally and theoretically *ab initio* calculation study. They noted that the protic solvents and methanol have a special ability to make the amide I band strongly redshifted or disappeared, due to the hydrogen bonding interaction between NMA and surrounding protic solvent molecules.[6] They also reported the hydrogen bonding strengths and conformations of NMA–water clusters.[4,5] However, the frequency shift mechanisms and the excited state structure information have not been reported in these studies. Therefore, the investigation of solvent dependence of peptides, especially the solvent dependence of C=O in simplest model molecules, seems prominently important for circumventing the excited state structure information.

Nearly half a century ago, the decrease in the C=O Raman wavenumber of acetone in aqueous solutions was reported.[8] This wavenumber deviation was mainly attributed to the hydrogen bond formation between the C=O group of the acetone and the OH group in the aqueous solvents.[9] In this

a)Author to whom correspondence should be addressed. Electronic mail: zdwhg@163.com. Tel.: 86-571-8684-3627. FAX: 86-571-8684-3627.
b)Author to whom correspondence should be addressed. Electronic mail: zhengxuming126@126.com. Tel.: 86-571-86843699. FAX: 86-571-86843702.

regards the C=O stretching ($\upsilon_{C=O}$) bands can be used as spectral probes to investigate the interaction and local orientation functional groups incorporated in macromolecules by monitoring their bands in shifts. However, while it is relatively easy to find molecules possessing solvent-sensitive properties, it is not always possible to provide an unambiguous interpretation of the origin of this solvent dependence.

It has been considered that two major mechanisms cause a wavenumber shift of the $\upsilon_{C=O}$: hydrogen bonding[10] and transition dipole coupling.[11] Some studies have suggested that hydrogen bond formation will result in negative values of the non-coincidence effect and be responsible for the decrease in the vibrational wavenumber of the carbonyl stretching mode.[10] On the other hand, it is known that a Raman active vibration can couple via the transition dipole to the same vibration in a neighboring molecule if some degree of short-range order exists due to the large permanent dipole moments of the molecules.[11] This causes a shift of wavenumbers of the isotropic Raman and anisotropic Raman components υ(aniso)-υ(iso) in a vibrational band, namely, non-coincidence effect.

Resonance Raman spectroscopy (RRS) provides overwhelming superiorities over the other spectroscopy techniques with the privilege to yield precious structural and conformational information of organic compounds.[12,13] Moreover, analyses of Raman excitation profiles (REPs) may also be helpful in getting precious information such as symmetry properties, displacements of the potential energy minimum, etc., of excited electronic states of molecules.[14,15] Comparative studies on the Raman excitation profiles of different solvents with respect to that of the ground state are very supportive in this regard.

In the present investigation, a detailed exploration of the electronic spectra and the solvent effects on the experimentally observed Raman intensity of bis(2-thienyl)ketone has been carried out and the Raman excitation profiles of different Raman bands obtained from different solvent have been compared and critically analyzed. Computational chemical methods may be carried out to better understand vibrational spectra, Herein, density functional theory (DFT) calculations were carried out using the hybrid B3LYP functional to aid vibrational mode assignments. These studies are expected to be helpful in understanding the photophysical and photochemical characteristics of the molecule.

II. EXPERIMENTAL AND COMPUTATIONAL METHODS

A. Resonance Raman experiments

The methods and experimental apparatus used for the resonance Raman experiments have been described elsewhere,[13,16] so only a short account will be given here. The harmonics of a nanosecond Nd:YAG laser and their hydrogen Raman shifted laser lines were used to generate the 252.7, 266.0, 282.4, 309.1, and 319.9 nm excitation wavelengths employed in the resonance Raman experiments. Spectroscopic grade solvents such as cyclohexane, methanol, and acetonitrile, are purchased from Sigma. Concentrations of the bis(2-thienyl)ketone (99% purity, Sigma) solutions are maintained from approximately 0.002 M to 0.006 M for RR spectra and 0.0001 M to 0.0003 M for the electronic absorption spectra. A lower power was used during the resonance Raman measurements to avoid saturation effects and other problems associated with high peak powers. A backscattering geometry was used for sample excitation and for collection of the Raman scattered light by reflective optics that imaged the Raman scattered light through a polarizer and entrance slit of a 0.5 m spectrograph. The grating of the spectrograph dispersed the light onto a liquid nitrogen cooled charge coupled device (CCD) mounted on the exit of the spectrograph, and the CCD acquired the Raman signal for about 90–150 s before being read out to an interfaced personal computer. The Raman shifts of the resonance Raman spectra were calibrated using the known vibrational frequencies of the solvent Raman bands. The solvent Raman bands were subtracted from the resonance Raman spectra using an appropriately scaled solvent spectrum. The Fourier transform (FT) IR and FT-Raman spectra of bis(2-thienyl)ketone in the neat solid phase were acquired to help assign the resonance Raman spectra.

The spectra of an intensity calibrated deuterium lamp were used to correct the resonance Raman spectral intensities for the variation in detection efficiency as a function of wavelength and portions of the resonance Raman spectra were fitted to a base line plus a sum of Lorentzian bands to find the integrated areas of the Raman bands.

B. Computational methods

In this work, we present a time-dependent density functional theory (TD-DFT) study of the prototype molecule bis(2-thienyl)ketone. The experimental RR spectra exhibit a marked dependence with respect to the polarity of the solvent. In order to simulate these effects, the solvent has been described by the polarizable continuum model (PCM) and the DFT[17] were done to determine the optimized geometry and vibrational frequencies as well as the electronic transition energies for the ground or excited electronic states in gas phase, solid state, in cyclohexane, methanol, and acetonitrile solution individually. In addition, we also performed the vibrational frequencies calculation for bis(2-thienyl)ketone-$(methanol)_{1,2}$ complex to explore how the hydrogen bond influence on the C=O vibrational frequency. Vibration wavenumber determination were computed by using the B3LYP/6-311G* level of theory for the ground state of bis(2-thienyl)ketone with a C_1 symmetry, while the electronic transition energies were calculated using B3LYP-TD/6-311G*. All of the DFT calculations made use of the GAUSSIAN 03 program software suite.[18]

C. Raman excitation profiles

The REPs are a plot of Raman band intensities versus excitation wavelengths. Intensities were determined from the measured peak height ratio I_N/I_S for the bands of the sample (N) and internal standard (S) using

$$\sigma_N = \sigma_S\,(I_N/I_S)\;[(\nu_0 - \nu_S)/(\nu_0 - \nu_N)]^4(C_S/C_N),$$

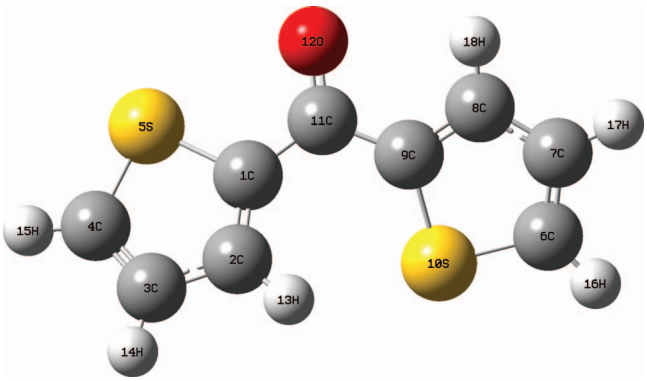

FIG. 1. Structure and atom labeling scheme of bis(2-thienyl)ketone.

where σ_N and σ_S are the absolute Raman cross sections of the band being determined and of the internal standard band, respectively, C_S/C_N is the concentration ratio, ν_0 is the laser excitation frequency, ν_N and ν_S are the vibrational frequencies of the sample and standard Raman bands, respectively. In this study, we mainly utilized solvent as an internal standard. The σ_S value for the 802 cm^{-1} mode of cyclohexane, 2249 cm^{-1} mode of acetonitrile was previously determined.[19]

III. RESULTS AND DISCUSSION

A. Molecular geometry of bis(2-thienyl)ketone

The molecular structure of bis(2-thienyl)ketone shown in Fig. 1 has been optimized by *ab initio* DFT levels of theories and by allowing relaxation of all the parameters, calculation has been found to converge to optimized geometry, which corresponds to the true energy minimum, as revealed by the absence of negative values in the calculated wavenumbers of the vibrational modes. Subsequently, the global minimum energy obtained for structure optimization of bis(2-thienyl)ketone with 6-311G* basis set is found to be approximately −1218.111 a.u. for DFT theory in gas phase. Selected optimized parameters of the molecule in gas phase, in cyclohexane, in methanol, and in acetonitrile solutions are presented in Table I for minimum energy geometry. The visual inspection with the use of GAUSSVIEW 3.0 helps us to estimate the dihedral angles (which are also included in the Table I).

Analysis of Table I allows some conclusions to be made. First, the bond length C=O, C–S, and C–C (except for C_6–S_{10} and C_7–C_8) systematically increase when medium polarity getting stronger while for the bond length C–H, C1–C11, and C9–C11 systematically decrease when the medium solvent getting more polar. These may be explained in terms of the facts that the stronger induced polarity of bis(2-thienyl)ketone may induced in the stronger medium polarity. Second, the dihedral angles of $C_1C_{11}O_{12}C_9$ approximate to 180°, and the dihedral angles of ring 1 and ring 2 are both approximate to zero. In the mean time the dihedral angles of $C_1C_{11}O_{12}C_9$ becomes bigger when the solvent polarity becomes stronger, which means that the geometry of carbonyl group C1(C11=O)C9 becomes more planar, while the geometry of ring 1 and ring 2 are all maintain roughly planar but shows a little tilt. Third, the dihedral angle between the ring 1 plane and the ring 2 plane calculated from the dihedral angles of $D(C_2C_1C_{11}O_{12})$ and $D(C_8C_9C_{11}O_{12})$ show that, the dihedral angles of ring 1 and ring 2 increased from 36.8° to 38.7° following with the solvent changed from gas to acetonitrile.

B. Vibrational analysis

In regard to the above structural information, the molecule of our interest, bis(2-thienyl)ketone, belongs to the

TABLE I. Equilibrium geometry of bis(2-thienyl)ketone in internal coordinate system.

	Ring 1	Gas phase	In C_6H_{12}	In CH_3OH	In CH_3CN	Ring 2	Gas phase	In C_6H_{12}	In CH_3OH	In CH_3CN
Selected atomic distance (Å)										
$R_{CC/CS}$	$R(C_1–S_5)$	1.8192	1.8204	1.8235	1.8236	$R(C_6–S_{10})$	1.7944	1.7946	1.7946	1.7946
	$R(C_4–S_5)$	1.7895	1.7904	1.7928	1.7928	$R(C_9–S_{10})$	1.8264	1.8269	1.8276	1.8277
	$R(C_3–C_4)$	1.3657	1.3658	1.3658	1.3658	$R(C_6–C_7)$	1.3641	1.3646	1.3658	1.3658
R_{CH}	$R(C_2–H_{13})$	1.0779	1.0785	1.0803	1.0802	$R(C_8–H_{18})$	1.0787	1.0799	1.0820	1.0820
	$R(C_3–H_{14})$	1.0794	1.0804	1.0822	1.0823	$R(C_7–H_{17})$	1.0794	1.0804	1.0823	1.0823
	$R(C_4–H_{15})$	1.0754	1.0767	1.0794	1.0795	$R(C_6–H_{16})$	1.0753	1.0767	1.0794	1.0794
R_{CX}	$R(C_1–C_{11})$	1.4623	1.4610	1.4584	1.4583	$R(C_9–C_{11})$	1.4722	1.4698	1.4654	1.4654
Selected atomic angles (deg)										
$A_{CCC/CCS/CSC}$	$A(S_5C_1C_2)$	110.60	110.54	110.44	110.43	$A(S_{10}C_9C_8)$	110.05	110.05	110.06	110.07
$A_{CCH/SCH}$	$A(C_1C_2H_{13})$	123.05	123.15	123.35	123.37	$A(C_9C_8H_{18})$	120.81	121.12	121.58	121.59
$A_{CCX/SCC}$	$A(S_5C_1C_{11})$	116.86	117.06	117.34	117.30	$A(S_{10}C_9C_{11})$	125.67	125.30	124.72	124.72
	$A(C_2C_1C_{11})$	132.46	132.31	132.13	132.17	$A(C_8C_9C_{11})$	124.17	124.54	125.10	125.09
Substitute atomic distance (Å)										
R_{CO}	$R(C_{11}–O_{12})$	1.2584	1.2613	1.2670	1.2670					
Atomic angles (deg)										
A_{CCO}	$A(C_1C_{11}O_{12})$	119.76	119.76	119.69	119.68	$A(C_9C_{11}O_{12})$	118.23	118.41	118.67	118.66
Dihedral angles (deg)										
D_{CCOC}	$D(C_1C_{11}O_{12}C_9)$	179.58	179.68	179.87	179.87	$D(C_9C_{11}O_{12}C_1)$	−179.58	−179.68	−179.87	−179.87

[a]*Note.* Calculation method B3LYP/6-311G* for gas phase; PCM for others.

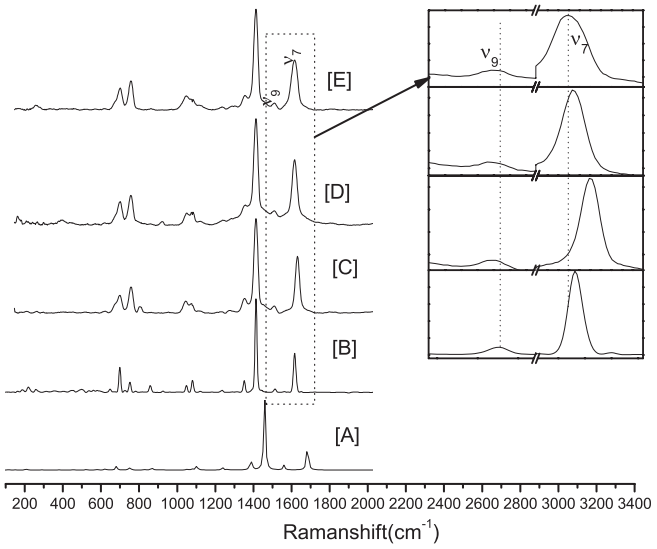

FIG. 2. Raman spectra of bis(2-thienyl)ketone (A) simulated Raman spectra within the frame work of DFT levels of theory with B3LYP/6-311G* basis set. Experimental Raman spectra with excitation wavelength 309.1 nm (B) in crystal state, (C) in cyclohexane, (D) in acetonitrile, and (E) in methanol solutions. Asterisks indicate respective solvent bands.

lowest symmetry C1 along with the two sulfur atoms placed asymmetrically with respect to the carbonyl group and the angle between two ring planes is about 37°. In the case of previous reported study on benzophenone molecule,[15] it was estimated from the same levels of theoretical calculations that the two phenyl rings have been placed symmetrically with respect to C_RCC_R plane keeping an angle of about 60° between them. Thus, it is proposed that in the ground state this molecule is more planar than its parent molecule benzophenone. The loan pair electrons of sulfur atoms are useful for electron transfer process in different types of photophysical and photochemical reactions.

We have carried out DFT frequency calculations for bis(2-thienyl)ketone in order to help elucidate the vibrational bands observed in the experimental FT-Raman and FTIR spectra of bis(2-thienyl)ketone as well as in the resonance Raman spectra of bis(2-thienyl)ketone. The 18 atoms of bis(2-thienyl)ketone give rise to 48 normal modes of vibration. Obviously, all the vibrations are expected to be both Raman and IR active. The observed 309.1 nm resonance Raman spectra of the sample in different environments are described in Fig. 2 along with the theoretically calculated DFT spectra. The vibrational wavenumbers of bis(2-thienyl)ketone in crystal form and in different solutions along with their IR counterparts are included in Table II. Theoretical bands calculated form DFT levels of theory are also included in this table in separate columns. Theoretically obtained IR spectra are compared with the experimental spectra of the compound and are shown in Fig. 3. It is to be emphasized that the calculated wavenumbers correspond to vibrational signatures of the molecule in its gas phase. Hence, the experimentally observed spectra of the solid and solution may differ to some extent from the calculated spectrum. In the DFT calculation, the B3LYP function tends to overestimate the wavenumbers of the fundamental modes compared to the experimentally observed values due to the combination of electron correlation effects and basis set deficiencies. In order to obtain a considerably better agreement with the experimental data, scaling factor has to be used. The wavenumbers of the C–H stretching vibrations are scaled down by the factors of 0.9594 for DFT analyses, whereas for all other vibrations a uniform linear scaling function of 0.9504* calculated +25.9095 has been applied.[20,21] Therefore, DFT vibrational wavenumbers presented in Table II have been linear scaled by the scaling function of 0.9504* calculated +25.9095.

Nevertheless, after applying the scaling factor, the theoretical calculation reproduces the experimental data well. The observed slight disagreement between the theory and the experiment may be attributed to anharmonicity. Besides, it is well known that the general tendency of the quantum chemical methods is to overestimate the force constants at the exact equilibrium geometry.[22]

For a proper understanding of IR and Raman spectra, a reliable assignment of all vibrational bands is essential. In this part of vibrational analysis, benzophenone[15] is considered as the parent molecule. The notations and assignments of the vibrations are based on the visualization GAUSSVIEW software, previous studied on the Raman spectra of 2,2-dipyridylketone were used as valuable references.[21] Figure 4 shows the Cartesian displacements of some selected vibrations considered from DFT calculation.

The FT-Raman and FT-IR spectra of bis(2-thienyl)ketone are shown in Fig. 3 and summarize in Table II. Spectra of bis(2-thienyl)ketone consist of A symmetry, which are allowed according to the selection rules of the *C*1 point group. These modes carry the A1 A2 B1 B2 symmetry label in *C*2*V* point group, applicable in case of the benzophenone. In bis(2-thienyl)ketone, splitting of the A symmetry modes can be interpreted in terms of point group symmetry of the molecule, because of the fact that there are two thiophene rings in bis(2-thienyl)ketone. These two thiophene rings have a different orientation relative to the carbonyl group. Therefore, corresponding to the *trans* position, the spectra bands theoretical (DFT) calculation for benzophenone were split into pairs of bands for bis(2-thienyl)ketone. The Raman band at 1414 cm^{-1} is assigned as the ring breathing mode (in-phase triangular mode) for both the rings, though the FT-IR and DFT removes this degeneracy, two bands are observed near 1400 cm^{-1} both in IR spectra and DFT calculation. The in plane C–H bending mode is observed at slightly higher frequency at 1224 and 1234 cm^{-1} for the two rings. The C–H wagging mode is observed at 698 and 721 cm^{-1} for the two rings. Other two $\beta_{CH(I,II)} + \nu_{AsC(1)C(11)\,C(9)} + \nu_{C(2)C(3)} + \nu_{C(7)C(8)}$ vibrations appear in the 1350 and 1325 cm^{-1} region. The remaining assignments of the two thiophene rings and of the carbonyl group of the molecule are in accordance with those reported elsewhere.[15,21,23]

Table II and Fig. 2 show the Raman shift contrast of the C=O stretching mode $\boldsymbol{\nu_7}$ for bis(2-thienyl)ketone in cyclohexane, methanol, and acetonitrile solution. The Raman shift of the solute molecule in the solutions is in general determined both by interactions between the solute molecules and by interactions between solute and solvent molecules. When the solute-solute mechanisms dominate, the dilution effect

TABLE II. Assignment of observed and calculated vibrational wavenumbers (in cm^{-1}) ν-stretching, α-in plane ring bending, β-in-plane bending, γ-wagging, δ-in-plane substitute bending, φ-torsion, I-S(5) ring, II-S(10) ring.

	Mode	Raman					DFT				Assignment
	(C1)	Solid	C_6H_{12}	CH_3OH	CH_3CN	IR	PCM scaled[a]	PCM calcuated	$1CH_3OH$[b]	$2CH_3OH$[c]	
A	ν_1						3110	3242	3241	3243	$\nu_{C(6)H}$
	ν_2						3109	3240	3240	3242	$\nu_{C(4)H}$
	ν_3	3106					3097	3228	3229	3230	$\nu_{CH(II)}$
	ν_4	3101				3097	3097	3228	3210	3214	$\nu_{CH(I)}$
	ν_5	3082				3080	3075	3205	3205	3207	$\nu_{CH(II)} + \beta_{CC(II)}$
	ν_6						3074	3204	3189	3200	$\nu_{CH(I)} + \beta_{CC(I)}$
	ν_7	1616	1627	1614	1609	1612	1626	1683	1651	1626	$\nu_{CO} + \nu_{C(2)C(3)} + \nu_{C(8)C(9)}$
	ν_8		1578				1513	1565	1563	1559	$\beta_{CH} + \nu_{C(1)C(2)} + \nu_{C(3)C(4)} + \nu_{C(6)C(7)} + \nu_{C(8)C(9)} + \nu_{AsC(1)C(11)\,C(9)}$
	ν_9	1514	1505.8	1510	1506	1514	1509	1560	1559	1556	$\beta_{CH(II)} + \nu_{C(6)C(7)} + \nu_{C(8)C(9)}$
	ν_{10}	1414	1411	1406	1402	1417	1413	1459	1460	1458	Ring breathing$_{(II)} + \beta_{CH(II)}$
	ν_{11}					1392	1412	1458	1458	1454	Ring breathing$_{(I)} + \beta_{CH(I)}$
	ν_{12}	1352		1352		1350	1350	1393	1395	1396	$\beta_{CH(I,II)} + \nu_{AsC(1)C(11)\,C(9)} + \nu_{C(2)C(3)} + \nu_{C(7)C(8)}$
	ν_{13}					1325	1343	1386	1386	1386	$\beta_{CH(I,II)} + \nu_{SynCS(I)}$
	ν_{14}			1284	1279	1290	1256	1294	1309	1314	$\beta_{CH(II)} + \nu_{AsC(1)C(11)\,C(9)}$
	ν_{15}	1234				1234	1227	1264	1265	1264	$\beta_{CH(I)}$
	ν_{16}					1224	1203	1238	1255	1256	$\beta_{CH(II)}$
	ν_{17}					1120	1104	1134	1137	1141	$\beta_{CH(I,II)} + \nu_{SynC(1)C(11)\,C(9)}$
	ν_{18}						1081	1110	1110	1111	$\beta_{C(3)H}\beta_{C(4)H}\beta_{C(6)H}\beta_{C(7)H}$
	ν_{19}	1080				1082	1071	1100	1103	1105	$\beta_{C(2)H}\beta_{C(4)H}\beta_{C(6)H}\beta_{C(8)H}$
	ν_{20}	1049				1049	1051	1078	1087	1090	$\beta_{CH(I,II)}$
	ν_{21}						1027	1053	1071	1074	$\beta_{C(2)H}\beta_{C(3)H}\beta_{C(7)H}\beta_{C(8)H} + \nu_{SynC(1)C(11)\,C(9)}$
	ν_{22}	925		920		924	910	930	991	965	$\gamma_{CH(II)}$
	ν_{23}						894	913	917	918	$\gamma_{CH(I)}$
	ν_{24}						866	884	886	887	$\beta_{C(2)\,C(3)C(4)} + \gamma_{CH(II)}$
	ν_{25}	858	860	855	841	860	850	867	883	881	$\gamma_{CH(I,II)}$
	ν_{26}						848	865	866	868	$\gamma_{CH(II)}$
	ν_{27}						833	849	853	854	$\gamma_{CH(I)}$
	ν_{28}	781				781	815	830	835	838	Ring breathing $+ \beta_{CO}$
	ν_{29}	752	743	748	738	744	742	753	758	757	$\gamma_{CH(I,\,II)} + \gamma_{OC}$
	ν_{30}						742	753	752	753	$\gamma_{CH(I,\,II)} + \gamma_{OC}$
	ν_{31}	727				731	735	746	746	747	$\gamma_{CH(I,\,II)} + \gamma_{OC} + \nu_{AsynCS}$
	ν_{32}					721	712	722	724	728	$\gamma_{CH(I)}$
	ν_{33}	698	691	696	705	698	705	714	721	724	$\gamma_{CH(II)}$
	ν_{34}	649				648	673	681	683	684	Ring breathing(I)
	ν_{35}						617	622	621	623	Ring breathing(II)
	ν_{36}	578				578	577	580	584	585	$\gamma_{CH(I,II)}$
	ν_{37}	561				559	568	570	572	571	$\gamma_{CH(I,II)}$
	ν_{38}						523	523	528	531	$\gamma_{CH(I,II)} + \beta_{C(1)C(11)\,C(9)}$
	ν_{39}	499					464	461	463	464	$\gamma_{CS(I,II)}$
	ν_{40}	455		474		455	455	451	452	452	$\gamma_{CS(I,II)}$
	ν_{41}						388	381	389	398	β_{CO}
	ν_{42}	258					298	286	291	293	δ(II)
	ν_{43}						226	210	223	221	δ(I)
	ν_{44}	218	235	235	235		218	202	210	211	γ_{CC} in CCS
	ν_{45}	187					172	154	165	178	$\gamma_{CH(I,II)} + \gamma_{CO}$
	ν_{46}	164					135	115	116	119	δ(I,II)
	ν_{47}						72	48	64	72	ϕ_{CC} in C(1)C(11)C(9)
	ν_{48}						65	41	42	50	ϕ_{CC} in C(1)C(11)C(9)

[a]Scaling factors for DFT are Y = 25.9095 + 0.9504*X for the region (36–1700 cm^{-1}) and 0.9594 for the region (3000–3300 cm^{-1}), respectively. Calculated method: DFT B3LYP/6-311G*.

[b]Vibrational frequencies calculated for bis(2-thienyl)ketone-(methanol) complex.

[c]Vibrational frequencies calculated for bis(2-thienyl)ketone-(methanol)$_2$ complex.

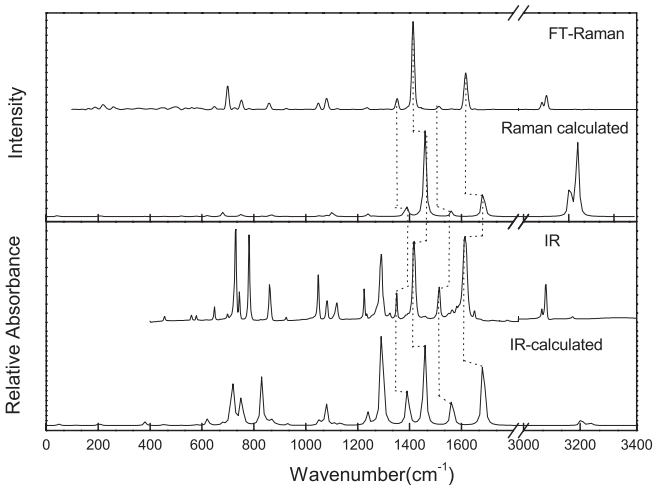

FIG. 3. The correlation of experimental FT-Raman and FT-IR spectra of bis(2-thienyl)ketone with the DFT simulated Raman and IR spectra under B3LYP/6-311G* basis set.

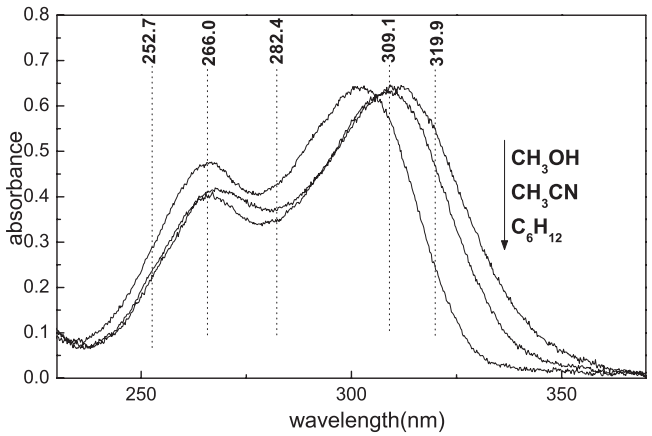

FIG. 5. Steady state electronic absorption spectra of bis(2-thienyl)ketone in methanol, cyclohexane, and acetonitrile environments, respectively.

will simply increase the intermolecular distance of the solute molecules and, hence, induce changes in the vibrational wavenumber owing to the weakened interactions. The Raman shift of the C=O stretching mode ν_7 of bis(2-thienyl)ketone increases in non-polar cyclohexane solvents and decrease in polar solvents acetonitrile or methanol. However, if the solute and solvent can form hydrogen bonds, then the Raman shift dependence of the vibrational wavenumber will be determined by the competition of two opposite effects: the dilution effect mentioned above, which will increase the vibrational wavenumber,[11] and the solvation and hydrogen bond effect, which will decrease the vibrational wavenumber when the solvation effects or hydrogen bond is formed or is being replaced by stronger effects.[10] In accordance with this interpretation for the hydrogen-bonded solutions, such as ketone methanol mixtures, we implicitly assume that all interactions, except the hydrogen bond effect, will be weakened by dilution, and that stronger hydrogen bond formation, if any, is the major mechanism responsible for the decrease of the C=O Raman shift ν_7. Therefore, the vast increase of the Raman shift ν_7 in the cyclohexane solution shown in Table II and Fig. 2 can be attributed to the constructively effect of the dilution, and the Raman shift in the methanol solution can be attributed to the combined effect of both the dilution and the formation of ketone-methanol hydrogen bonds. Consequently, we would also expect that the C=O Raman shift ν_7 of the bis(2-thienyl)ketone in acetonitrile solutions should be related to the relative strength of the dilution and ketone-acetonitrile solvation. Based on these arguments, a further discussion of the observed C=O Raman shifts ν_7 in the bis(2-thienyl)ketone-methanol and bis(2-thienyl)ketone-acetonitrile solutions is presented below. The most obvious evidence for the competition between the salvation or hydrogen bond effect and the dilution effect is the C=O Raman shift ν_7 in the bis(2-thienyl)ketone solution shown in Fig. 2. Obviously the situation for bis(2-thienyl)ketone-methanol solution the hydrogen bond dominates the effects while for bis(2-thienyl)ketone-acetonitrile the two opposite effects of dilution and salvation get to a close match.

In order to exam the hydrogen bond solely influence on the C=O Raman shifts ν_7, we have also performed the vibrational frequencies calculation for bis(2-thienyl)ketone-$(methanol)_{1,2}$ complex, which is included in the Table II. From Table II we can know that the hydrogen bond in bis(2-thienyl)ketone-$(methanol)_2$ complex really effectively reduced the C=O vibrational frequency, which is in good consistent with the literature.[10]

The Raman shift ν_9 in Table II decrease in both the non-polar solvent cyclohexane and polar solvents acetonitrile or methanol. It is a very week broad peak and shows big uncertainty in the absolute wavenumber of the C=O centroid. Also, Fermi resonance interaction should be considered for the reduction Raman shift of ν_9 involving the single C=O vibration fundermental ν_9 (1514 cm^{-1}) vibrational coupling with the overtone $2\nu_{29}(752 \times 2\ cm^{-1})$.

1. Absorption spectrum

Figure 5 presents the absorption spectrum of bis(2-thienyl)ketone in cyclohexane, methanol, and acetonitrile solutions with the wavelengths for the resonance Raman experiments indicated above the spectrum. Table III lists the B3LYP-TD/6-311G* computed electronic absorption spectrum, the corresponding electric dipole transition orbitals, the oscillator strengths, and the description of molecular orbital associated with the dominant one electronic vertical

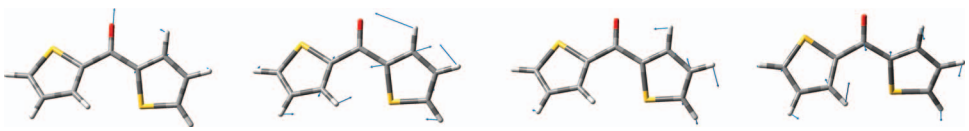

FIG. 4. Cartesian displacements (DFT//B3LYP/6-311G*) of some selective vibrational modes of bis(2-thienyl)ketone.

TABLE III. Experimental electronic absorption bands and theoretical /TD-DFT/6-311G*/ vertical one-electron excitations in different environments. Only CI expansion coefficients with absolute value 0.2 are shown in the table.

	Theo gas phase				Cyclohexane					Methanol					Acetonitrile					
	Band		Molecular orbital		Band (nm)			Molecular orbital		Band (nm)			Molecular orbital		Band (nm)			Molecular orbital		
Sl no.	(nm)	f	excitation	CI co-eff.	Theo.	Expt.	f	excitation	CI co-eff.	Theo.	Expt.	f	excitation	CI co-eff	Theo.	Expt.	f	excitation	CI co-eff.	Transitions
1	344		46 → 51	0.3883	341		00.0006	46 → 51	0.4916	336		0.0010	46 → 51	0.5355	336		0.0007	46 → 51	0.5338	
			48 → 51	0.3041				48 → 51	0.2370				49 → 51	0.3592				49 → 51	0.3654	
			49 → 51	0.3496				49 → 51	0.3657											
2	303	0.2919	49 → 51	−0.3082	305	301	0.2990	50 → 51	0.6193	309	312	0.3104	50 → 51	0.6322	309	309	0.3103	50 → 51	0.6363	$G \rightarrow S_1$
			50 → 51	0.5787				49 → 51	−0.2132											
3	284	0.0030	46 → 51	−0.3746	285		0.0028	46 → 51	0.4212	287		0.0025	46 → 51	−0.3932	287		0.0027	46 → 51	−0.4006	
			47 → 51	0.3257				47 → 51	−0.2081				47 → 51	0.3321				47 → 51	0.3150	
			49 → 51	0.3667				48 → 51	−0.2088				49 → 51	0.4057				49 → 51	0.4034	
			50 → 51	0.2114				49 → 51	−0.3965											
4	275	0.0177	46 → 51	0.3428	277		0.0213	46 → 51	0.2049	282		0.0268	47 → 51	0.4216	282		0.0269	47 → 51	0.4818	
			47 → 51	0.5358				47 → 51	0.6327				48 → 51	0.4956				48 → 51	0.4412	
5	270	0.0698	46 → 51	−0.2292	271	267	0.0675	48 → 51	0.5769	273	267.6	0.0654	47 → 51	−0.3959	273	267	0.0650	47 → 51	−0.3428	$G \rightarrow S_2$
			48 → 51	0.5430				49 → 51	−0.2679				48 → 51	0.4061				48 → 51	0.4506	
			49 → 51	−0.2373									49 → 51	0.2960				49 → 51	0.2983	
6	233	0.0499	46 → 52	0.2306	231		0.0552	46 → 52	0.2592	229		0.0628	46 → 52	0.2276	229		0.0627	46 → 52	0.2265	
			49 → 52	0.5723				49 → 52	0.6103				49 → 52	0.6363				49 → 52	0.6379	
			50 → 52	0.2213																

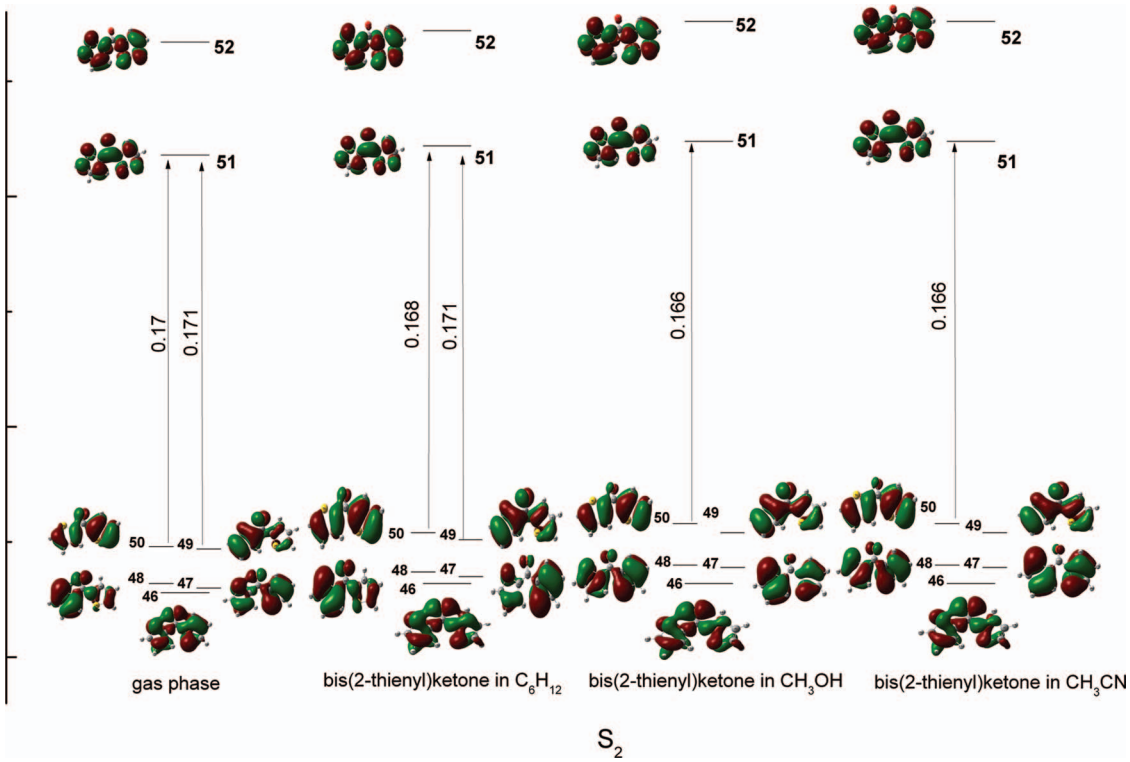

FIG. 6. Comparison of five highest occupied and two lowest unoccupied orbitals for the A absorption band of bis(2-thienyl)ketone in gas phase, cyclohexane, methanol, and acetonitrile environments, respectively.

transition for bis(2-thienyl)ketone. Table III shows that among the calculated electronic transitions above 230 nm optical region there are two transition-allowed absorption bands at 305 and 271 nm (A- and B-band with the oscillator strength of $f = 0.2990$ and 0.0675, respectively) in cyclohexane solution. This is in good agreement with the intense experimental absorption band at 303.0 and 267 nm (A- and B-band with the experimental oscillator strength of $f = 0.31$ and 0.17, respectively) in cyclohexane solution. Experimentally, these two absorptions exhibit redshifts of 8.8 and 0.8 nm, respectively, in methanol solution, and redshifts of 7.6 and 0.2 nm, respectively, in acetonitrile solution. This was attributed to the fact that additional stabilization by the solvent electronic polarization is larger in the more polar ground state than the $\pi\pi^*$ state. This trend was corroborated by the spatial distribution of solvent electronic polarization around the solute carbonyl sites. The influence of the solvent electronic polarization becomes prominent in a polar solvent, though the overall blue shift is small.

The TD-DFT method predicts appreciable shift of energy for singlet G→S2 states in going from gas phase to solvent phases and the results are coincident with the experimental absorption spectra very well (Table III). The topologies of molecular orbitals may be considered as a guide to the TD-DFT analyses of the optical absorptions (Fig. 6). Figure 6 displays the seven orbitals associated with the electronic transition of the calculated A-band absorption. It shows that all the unoccupied and occupied orbitals energy were elevated by the solvents, but the elevation degree is different, the occupied orbitals energy were elevated more relative to the unoccupied ones, and this situation exhibits more remarkably in the polar solvent than that in the non-polar solvent. It means that the solvents could reduce the energy gap of the orbital transition from the highest occupied molecular orbital (HOMO) to lowest unoccupied molecular orbital (LUMO) and consequently lead to the red shift of the electronic transition band. The orbital topologies also show that all the unoccupied orbital with different solvent are of the same type and with minor energy difference while that for the occupied orbital are of very different electron cloud topography. Conclusions could be draw that the solvent dependant properties are mainly manipulated through the HOMO, HOMO-1, HOMO-2, and HOMO-3 orbital. The orbital topologies in Fig. 6 show that orbital 50 (HOMO) are π orbitals of C_1–C_2/C_3–C_4, and C_6–C_7/C_8–C_9–S_{10} bonding with electron cloud prevailing distributed over the C_6–C_7/C_8–C_9–S_{10} in gas phase while that with electron cloud average distributed over two rings in solutions. Similarly, the Orbital 49 (HOMO-1) in gas phase are π orbital with electron density being prevailing delocalized on C_2–C_1–S_5/C_3–C_4 over C_8–C_9/S_{10}–C_6–C_7 bonding while that in solutions are π orbitals delocalized averagely on C_2–C_1–S_5/C_3–C_4 and C_8–C_9/S_{10}–C_6–C_7 bonding. Contrast of the 50, 49, 48, and 47 orbital topologies between bis(2-thienyl)ketone in gas phase and in solution phase, the electronic density appears more dispersed and uniform in solution phase.

In a word LUMO orbital of the molecule are of π^* nature, whereas HOMO, HOMO-1, and HOMO-2 are enriched with contributions from π nature and spread over both the rings. The experimental 303 nm absorption band (A-band) in solution could be assigned as $\pi(C_1$–C_2/C_3–$C_4)$ → $\pi^*(C_1$–C_2/C_3–$C_4)$ and $\pi(C_6$–C_7/C_8–C_9–$S_{10})$ → $\pi^*(C_6$–C_7/C_8–C_9–$S_{10})$ transition. Our 319.9, 309.1 nm excitation

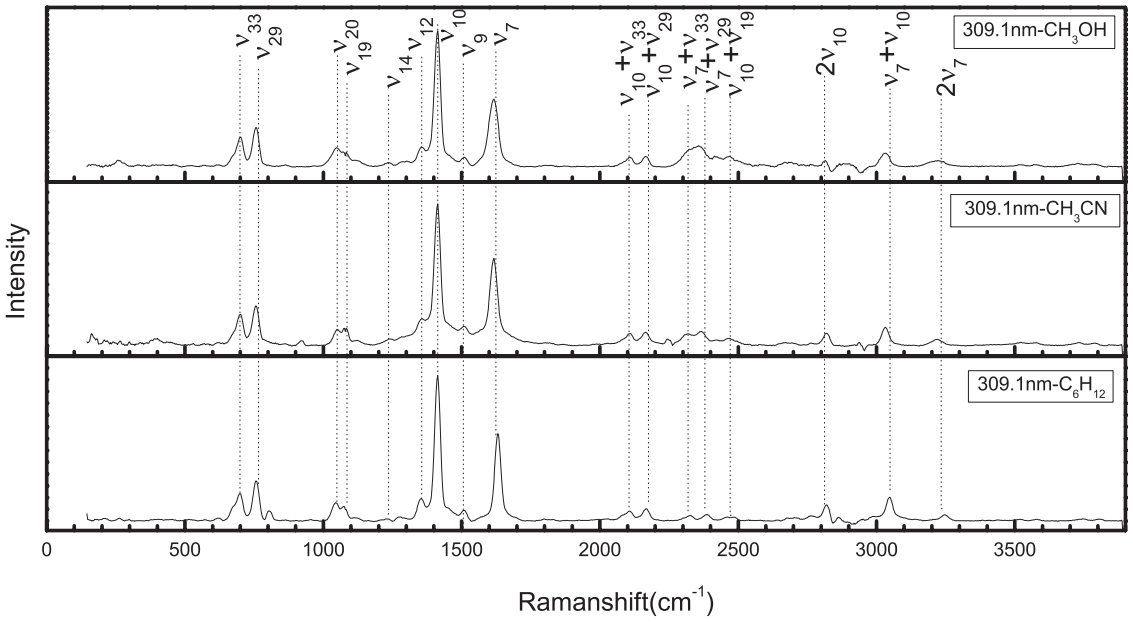

FIG. 7. Comparison of the 309.1 nm resonance Raman spectra of bis(2-thienyl)ketone in methanol, acetonitrile, and cyclohexane environments, respectively.

wavelengths used in the resonance Raman experiments should be mostly on resonance with the A-band absorption of bis(2-thienyl)ketone while 266.0, 252.7 nm excitation wavelengths is resonance with the B-band and 282.4 nm excitation wavelengths is resonance with the overlap absorption of A- and B-band. Since, the A-band transition transfers electron density from C_1–C_2/C_3–C_4 and C_6–C_7/C_8–C_9–S_{10} to C_{11} of carbonyl (see Fig. 6), a localized charge transfer nature is expectable for bis(2-thienyl)ketone in a short time upon absorbing 303 nm excitation. The molecular orbital coefficient analysis also supports the electron density redistribution.

2. Resonance Raman spectroscopy and Raman excitation profiles

We note first that since our laser line frequencies fall in the electronic absorption region (Fig. 5) we may expect to see resonant Raman effects.

In order to explore the solvent dependent variation of Raman intensity, sum-over-states approach has been utilized as discussed earlier. In the framework of Albrecht's theory, the Born-Oppenheimer approximation is employed to separate the vibronic states into products of electronic and vibrational states, and the transition dipole moments are expanded as a Taylor series in the nuclear coordinates. The Raman intensity, which are subject to enhancement when the incident radiation approaches a contour of an intense absorption band, get intensity contribution by either (i) Frank-Condon A-term, (ii) Herzberg-Teller B-term, or (iii) both.

Figure 7 displays the comparison of the 309.1 nm resonances Raman spectra of bis(2-thienyl)ketone in methanol, acetonitrile, and cyclohexane solutions. The spectra shown in Fig. 7 have been corrected for sample reabsorption as well as the wavelength dependence response of the detection system and the solvent Raman bands were removed from the spectra by subtracting an appropriately scaled solvent spectrum and regions of the solvent subtraction artifacts are indicated by asterisks. The dashed lines in Fig. 7 indicate the correlation of nine A_1 type fundamental vibrational modes labeled as υ_7, υ_9, υ_{10}, υ_{12}, υ_{14}, υ_{19}, υ_{20}, υ_{29}, and υ_{33} and several overtones and combination bands of 309.1 nm RRS of bis(2-thienyl)ketone in methanol, acetonitrile, and cyclohexane solutions. A total of 309.9 nm radiation is in the region of discrete vibronic transitions and is termed discrete resonance Raman scattering. Figure 7 shows that the resonance Raman patterns, including the wavenumbers and relative intensities of all the fundamental, combination bands, and overtones, show no distinct difference with increasing polarity of the medium. Most of the resonance Raman features in Fig. 7 can be assigned to the fundamentals, overtones, and combination bands of about four Franck-Condon active vibrational modes based on the information provided in Table II: the nominal ring breathing$_{(II)}$+$\beta_{CH(II)}$ stretch υ_{10} (1414 cm^{-1}), the nominal ν_{CO} + $\nu_{C(2)C(3)}$ + $\nu_{C(8)C(9)}$ stretch υ_7 (1616 cm^{-1}), the nominal $\gamma_{CH(I,\,II)}$ + γ_{OC} stretch υ_{29} (752 cm^{-1}), the $\gamma_{CH(II)}$ υ_{33} (698 cm^{-1}).

The normal modes υ_{10} [breathing + $\nu_{SynC(1)C(11)C(9)}$ stretch] and υ_7 [ν_{CO} + $\nu_{C(2)C(3)}$ + $\nu_{C(8)C(9)}$ stretch] get major intensity contribution for the bis(2-thienyl)ketone in all of the solvent from the 309.1 nm excitation (A-band absorption), which means that photoexcitation of bis(2-thienyl)ketone in the A-band absorption causes larger motions along the ring breathing$_{(II)}$ + $\beta_{CH(II)}$ stretch, ν_{CO} + $\nu_{C(2)C(3)}$ + $\nu_{C(8)C(9)}$ stretch, the $\gamma_{CH(I,\,II)}$ + γ_{OC} stretch, and the $\gamma_{CH(II)}$ and have not been influenced by the medium. It could be inferred that they get major intensity enhancement from the diagonal A-term of the scattering tensor through the S2 electronic state (A-band) (Table III). The diagonal A-term contributions from the relevant S2 states (A-band) for the above modes indicate that the relevant ring C–C bond, C=O bond, and $C_{(1)}C_{(11)}C_{(9)}$ asymmetric bond distances undergo appreciable change due to excitation from the ground to the respective excited states.

Thus, the electronic state S2 may be expected to have a good amount of charge transfer between the π charge cloud of the ring and the charges of the ketone group. The RRS patterns show that the polarity of the solvent has not change the photo-induced reorganization energy dissipation, the displacement for the S2 state and the photo relaxation reaction path.

The normal modes analysis is in coincidence with the TD-calculations and absorption spectrum (Fig. 5). The electronic transition associated with the A-band absorption is featured by the localized $\pi(C_1–C_2/C_3–C_4) \rightarrow \pi^*(C_1–C_2/C_3–C_4)$ and $\pi(C_6–C_7/C_8–C_9–S_{10}) \rightarrow \pi^*(C_6–C_7/C_8–C_9–S_{10})$ transition. Since the charge density at the site of the C=O group increases markedly after orbital transition from the HOMO to the LUMO, which inevitably strengthen the $C_{(1)}C_{(11)}C_{(9)}$ bond and weakens the $C_{(6)}–C_{(7)}/C_{(1)}–C_{(2)}$ bond (see orbitals 49 and 51 in Fig. 6), the $C_{(1)}C_{(11)}C_{(9)}$ bond shortening and $C_{(6)}–C_{(7)}/C_{(1)}–C_{(2)}$ bond lengthening is expected. This is consistent with the observed predominant overtone progressions of the nominal ring breathing$_{(II)}$ + $\beta_{CH(II)}$ stretch υ_{10} (1414 cm^{-1}) in 309.1 nm resonance Raman spectra in Fig. 7 and this also indicates that the molecule undergoes large excited state geometry structure change along $C_{(6)}–C_{(7)}/C_{(1)}–C_{(2)}$ and $C_{(1)}C_{(11)}C_{(9)}$ reaction coordinate. But the polarity of the solvent exerted its influence on differentiation the energy elevation of occupied and unoccupied orbits to reduce the energy gap of the orbital transition from the HOMO to LUMO and then lead to the redshift of the electronic transition band. TD-calculations show that the solvent dependant properties are mainly manipulated through the elevation of the energy of occupied ground electronic state.

Figure 7 shows that while the vibrational modes in wavenumber, in description, and in intensity patterns for different solvent resonance Raman spectrum are very similar, the band full-width at half-maximum (FWHM) for C=O stretching mode υ_7 is very different. The FWHM for band υ_7 is 37.5 cm^{-1} in methanol, 26.8 cm^{-1} in acetonitrile, 21.4 cm^{-1} in cyclohexane, and 15.4 cm^{-1} in pure solid state.

Devi *et al.*[24] have studied systematically the function between the bandwidth of C=O stretching vibration, the van der Waals' volume, and the solvent concentrations and found that repulsive type of intermolecular forces are responsible in the line broadening mechanism. The question of how to handle the solvent in analyzing and modeling resonance Raman intensities is still a matter of considerable debate. One proposal advanced a KHD-like equation in which the slow solvent degrees of freedom are included as inhomogeneous broadening at the Raman cross-section level while the fast solvent motions are included by replacing the simple exponential lifetime damping, $e^{-\gamma t}$, with the more general broadening function $e^{-g(t)}$. Solvent induced inhomogeneous broadening is nearly always treated as a Gaussian distribution of electronic zero-zero energies while homogeneous broadening is more in dispute. The solvent induced inhomogeneous broadening in this case may imply for the prolonged life time of S2 electronic state.

In order to quantitatively analysis the solvent effect on normal modes intensity in the resonance Raman spectrum, the observed REPs of several normal modes of vibration of bis(2-thienyl)ketone molecule in methanol, acetonitrile, and cyclohexane solutions are calculated and presented in Fig. 8. The observed profiles in 309.1 nm laser excitation at room temperature (around 30 °C) are presented. From the Fig. 8, the REPs of the individual normal modes are very close among the different solvent. The REPs of the fundamental, combination, and overtones of υ_7 seem different from others for the relative lower REPs in methanol solvent. This may ascribe to the strong hydrogen bond interactions between the solvent and solute molecules.

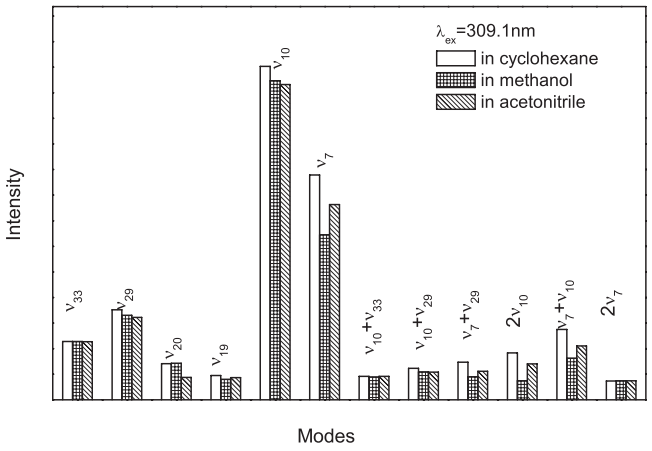

FIG. 8. Comparison of the REPs for several vibrational modes and combination modes obtained from the 309.1 nm resonance Raman spectra of bis(2-thienyl)ketone in methanol, acetonitrile, and cyclohexane environments, respectively.

See supplementary material for additional excitation wavelengths resonance Raman spectroscopy of bis(2-thienyl)ketone in different solvent to notice the C=O Raman shift.[25]

IV. CONCLUSION

The purpose of the paper is to confirm theoretically the experimental findings of the solvent effect on electronic energy levels, vibrational signals, and molecular geometry of bis(2-thienyl)ketone. The angle between the two ring planes is increased from 36.8° to 38.7° following with the solvent changed from gas to acetonitrile as found from DFT calculation, although the geometry of carbonyl group ($C_1C_{11}=OC_9$) becomes more planar. DFT is not only found to give reasonably good singlet vertical excitation energies vary with medium polarity and vibrational signatures of the molecule but are also compatible with the findings from the REP studies too. The Raman shift of the C=O stretching mode υ_7 of bis(2-thienyl)ketone increases in non-polar cyclohexane solvents and decrease in polar solvents acetonitrile or methanol. The results were interpreted through the dilution effect, solvation effects, and hydrogen bond-forming effects. DFT method is used to aid the accurate description of the vibrational frequencies for the ground state. 309.1(A-band) nm excitation wavelengths RRS for bis(2-thienyl)ketone in various solvents were acquired and the Raman effect was analyzed. Our results indicate that the short-time $S_0 \rightarrow S_2$ photo relaxation dynamics of bis(2-thienyl)ketone have substantial multidimensional character mainly in the nominal the ring breathing$_{(II)}$

$+ \beta_{CH(II)}$ stretch, $\nu_{CO} + \nu_{C(2)C(3)} + \nu_{C(8)C(9)}$ stretch and the $\gamma_{CH(I,II)} + \gamma_{OC}$ stretch, with smaller contributions from the nominal $\gamma_{CH(II)}$ and the polarity of the solvent has not change the photo-induced reorganization energy dissipation, the displacement for the S2 state and the photo relaxation reaction path. But the Raman shift of the C=O stretching mode ν_7 indicate the molecular symmetry changes of the excited S2 states relative to the ground states.

ACKNOWLEDGMENTS

This work was supported by grants from National Science Foundation of China (NSFC) (Grant No. 20703038), the National Basic Research Program of China (Grant No. 2007CB815203), and NSFZ (Grant Nos. Y407245 and R405465). H. Wang wishes to acknowledge the referees for their contributions in making this a better paper.

[1]O. V. Prezhdo and Y. V. Pereverzev, Acc. Chem. Res. **42**(6), 693 (2009).
[2]M. Bouchard and M. Auger, Biophys. J. **65**(6), 2484 (1993); Y. T. Lee, J. Raman Spectrosc. **28**(1), 45 (1997); L. Zhang, D. H. Quan, L. Wang, G. Z. Yang, and Y. X. Weng, Sci. China, Ser. G **47**(2), 208 (2004); C. T. Middleton, B. Cohen, and B. Kohler, J. Phys. Chem. A **111**(42), 10460 (2007); M. Hulko, F. Berndt, M. Gruber, J. U. Linder, V. Truffault, A. Schultz, J. Martin, J. E. Schultz, A. N. Lupas, and M. Coles, Cell **126**(5), 929 (2006); B. Kustner, C. Schmuck, P. Wich, C. Jehn, S. K. Srivastava, and S. Schlucker, Phys. Chem. Chem. Phys. **9**(32), 4598 (2007); S. Schlucker, J. Koster, R. K. Singh, and B. P. Asthana, J. Phys. Chem. A **111**(24), 5185 (2007); J. Chen and B. A. Barry, Photochem. Photobiol. **84**(3), 815 (2008); R. Gross, C. Schumann, M. M. N. Wolf, J. Herbst, R. Diller, N. Friedman, and M. Sheves, J. Phys. Chem. B **113**(22), 7851 (2009).
[3]G.-J. Zhao and K.-L. Han, Biophys. J. **94**, 38 (2008).
[4]L. C. Mayne and B. Hudson, J. Phys. Chem. **95**(8), 2962 (1991); L. M. Markham and B. S. Hudson, *ibid.* **100**(7), 2731 (1996).
[5]N. S. Myshakina, Z. Ahmed, and S. A. Asher, J. Phys. Chem. B **112**(38), 11873 (2008); Z. H. Chi, X. G. Chen, J. S. W. Holtz, and S. A. Asher, Biochemistry **37**(9), 2854 (1998).
[6]X. G. Chen, R. Schweitzerstenner, S. A. Asher, N. G. Mirkin, and S. Krimm, J. Phys. Chem. **99**(10), 3074 (1995); X. G. Chen, S. A. Asher, R. Schweitzerstenner, N. G. Mirkin, and S. Krimm, J. Am. Chem. Soc. **117**(10), 2884 (1995).
[7]G.-J. Zhao and K.-L. Han, J. Phys. Chem. A **111**, 2469 (2007); ChemPhysChem **9**, 1842 (2008); J. Phys. Chem. A **113**, 14329 (2009); G.-J. Zhao and K.-L. Han, "Hydrogen Bonding in the Electronic Excited State," Acc. Chem. Res. (in press).
[8]P. G. Puranik, Proc. Indian Acad. Sci., Sect. A **37**, 499 (1953).
[9]S. L. Wallen, L. Nikiel, Y. T. Lee, and J. Jonas, J. Raman Spectrosc. **26**(11), 1019 (1995).
[10]G. Eaton, M. C. R. Symons, and P. P. Rastogi, J. Chem. Soc., Faraday Trans. **85**, 3257 (1989); G. Eaton and M. C. R. Symons, *ibid.* **84**, 3459 (1988); G. Eaton, A. S. Penanunez, and M. C. R. Symons, *ibid.* **84**, 2181 (1988).
[11]M. Musso, M. G. Giorgini, H. Torii, R. Dorka, D. Schiel, A. Asenbaum, D. Keutel, and K. L. Oehme, J. Mol. Liq. **125**(2–3), 115 (2006); H. Torii, M. Musso, M. G. Giorgini, and G. Doge, Mol. Phys. **94**(5), 821 (1998); M. Musso, M. G. Giorgini, G. Doge, and A. Asenbaum, *ibid.* **92**(1), 97 (1997); H. Schulze, O. Ristau, and C. Jung, Eur. J. Biochem. **224**(3), 1047 (1994).
[12]P. C. Gao, H. G. Wang, K. M. Pei, and X. M. Zheng, Chem. Phys. Lett. **445**(4–6), 173 (2007); J. Xu, J. M. Wan, Y. Y. Zhao, M. Q. Lv, X. M. Zheng, G. D. Wang, and H. G. Wang, Spectrochim. Acta, Part A **75**(5), 1381 (2010); H. G. Wang, J. Xu, J. M. Wan, Y. Y. Zhao, and X. M. Zheng, J. Phys. Chem. B **114**(10), 3623 (2010).
[13]H. G. Wang, B. Liu, J. M. Wan, J. Xu, and X. M. Zheng, J. Raman Spectrosc. **40**(8), 992 (2009); H. G. Wang, B. Liu, Y. Y. Zhao, and X. M. Zheng, *ibid.* **40**(9), 1312 (2009).
[14]T. Mishra, A. K. De, S. Chattopadhyay, P. K. Mallick, and P. Sett, Spectrochim. Acta, Part A **61**(4), 767 (2005); C. B. Ruan, H. G. Wang, H. L. Zhu, X. M. Zheng, and D. L. Phillips, J. Chem. Phys. **129**(21), 214506 (2008); Y. Q. Wang, H. G. Wang, S. Q. Zhang, K. M. Pei, X. M. Zheng, and D. L. Phillips, *ibid.* **125**(21), 214506 (2006); S. Q. Zhang, H. G. Wang, K. M. Pei, X. M. Zheng, and D. L. Phillips, *ibid.* **126**(19), 194505 (2007).
[15]P. Sett, T. Misra, S. Chattopadhyay, A. K. De, and P. K. Mallick, Vib. Spectrosc. **44**(2), 331 (2007).
[16]W. M. Kwok and D. L. Phillips, Chem. Phys. Lett. **235**(3–4), 260 (1995).
[17]C. T. Lee, W. T. Yang, and R. G. Parr, Phys. Rev. B **37**(2), 785 (1988); A. D. Becke, J. Chem. Phys. **84**(8), 4524 (1986).
[18]M. J. Frisch, G. W. Trucks, H. B. Schlegel *et al.*, GAUSSIAN 13, Revision B.02, Gaussian, Inc., Pittsburgh, PA, 2003.
[19]B. Li and A. B. Myers, J. Phys. Chem. **94**(10), 4051 (2002); M. O. Trulson and R. A. Mathies, J. Chem. Phys. **84**(4), 2068 (1986).
[20]G. Rauhut and P. Pulay, J. Phys. Chem. **99**, 3093 (1995); G. Rauhut and P. Pulay, J. Am. Chem. Soc. **117**, 4167 (1995).
[21]P. Sett, T. Mishra, J. Chowdhury, M. Ghosh, S. Chattopadhyay, S. K. Sarkar, and P. K. Mallick, J. Chem. Phys. **128**(14), 144507 (2008).
[22]G. Rauhut and P. Pulay, J. Phys. Chem. **99**(10), 3093 (1995).
[23]X. F. Wu, X. M. Zheng, H. G. Wang, Y. Y. Zhao, X. G. Guan, D. L. Phillips, X. B. Chen, and W. H. Fang, J. Chem. Phys. **133**(13), 134507 (2010); H. G. Wang, S. S. Shen, L. B. Wang, and X. M. Zheng, J. Phys. Chem. B **114**(50), 16847 (2010).
[24]T. G. Devi, A. Das, and K. Kumar, Spectrochim. Acta, Part A **60**(1–2), 211 (2004).
[25]See supplementary material at http://dx.doi.org/10.1063/1.3697482 for 319.9, 282.4, 266 and 252.7 nm excitation wavelengths resonance Raman spectroscopy of bis(2-thienyl)ketone in crystal state, in cyclohexane, in methanol and in acetonitrile solutions, comparison of the FT-Raman, FT-IR, 319.9, 309.1, 282.4, 266.0 nm resonance Raman spectra, experimental and B3LYP /6-311G* computed vibrational frequencies of bis(2-thienyl)ketone.